Desalination, Volume 515, 1 November 2021, Article number 115211
DOI:10.1016/j.desal.2021.115211

Experimental study on three-effect tubular solar still under vacuum and immersion cooling

Tiantong Yan[a], Guo Xie[a,] *, Wenlong Chen[b], Zhanglin Wu[a], Jialing Xu[a], Yingzhang Liu[a]

[a] *State Key Laboratory of Hydraulics and Mountain River Engineering, College of Water Resource & Hydropower, Sichuan University, Chengdu 610065, China*

[b] *School of Water, Energy and Environment, Cranfield University, Cranfield MK43 0AL, UK*

**Corresponding author. Tel/Fax: +86-028-85405633*
E-mail address: 2008xieguo@scu.edu.cn (G. Xie)

Abstract

Solar still is widely used for supplying fresh water to small communities in remote areas. One drawback of this technique lies in the low freshwater yield. Recent studies on stills of multi-effect and vacuum design proved their potential for high yield. However, such systems suffer from high electricity consumption and insufficient cooling. In this study, a novel system with a periodic pressure control scheme and water immersion cooling has been proposed to mitigate these defects. A prototype was constructed and associated with a 0.19-m^2 solar panel. A 5-day outdoor experiment was conducted to evaluate the overall performance. Results indicated that the highest yield during the test was 9.8 kg/m^2 at operating pressure of 40 kPa. A significant performance ratio of 1.87 was achieved with immersion cooling, i.e., 0.42 higher than that with air cooling. Thermal analysis showed that the heat transfer coefficient of water immersion cooling was 15–50 times higher than that of air cooling. Compared with previous vacuum-operated systems, the specific electricity consumption of maintaining vacuum was greatly reduced, i.e., from 21.6 kJ/kg to 1.7 kJ/kg for the case at 60 kPa. The forecast cost of the distilled water is $0.012/kg, representing an affordable desalination technique for off-grid communities.

Keywords: Solar still; Vacuum; Immersion cooling; Multi-effect; Tubular; Electricity consumption

1 Introduction

The global fresh water shortage is one of the most pressing challenges to human society. It is estimated that two-thirds of the world population will experience water scarcity in 2025 [1]. In some water-starved regions, e.g., the Middle-East, desalination technique has been widely used to purify seawater into fresh water. Desalination is also recognized as a preferable method to alleviate the global water scarcity in the coming years. The desalination process consumes a huge amount of energy [2]. In recent years, much attention has been paid to solar desalination because of its environmentally friendly nature over the technique using fossil fuels. Various solar desalination devices have been developed since ancient times [3]. Conventional basin-type solar still, which consists of a water basin and a transparent cover, is one of the most common solar stills for its low cost and easy operation. However, the conventional solar stills are not so attractive in practical use due to their low productivity.

The productivity of solar distillation systems depends strongly on the temperature of saline water. Many methods have been proposed to increase the production by elevating the evaporation temperature in a still. One of the most common methods is coupling the still with a solar collector [4]. Manokar et al. [5] found that a basin solar still integrated with a flat solar collector yielded 45% more freshwater compared with that without a collector. Integration of a solar still with a parabolic concentrator increases the trough temperature by approximately 40 °C, and achieves a 676% productivity enhancement [6, 7] which is recently escalated to 890% by using gravel as heat storage material [8]. Many researchers tried to add solar absorbing materials into basin water to increase the solar energy harvest [9, 10]. Recently, solid materials with micro/nano structure have received much attention due to their high photothermal efficiency [11], yet the productivity remains low when these materials were applied. A large gap exists between high absorptivity materials and productive solar stills [12].

Vacuum operation is another effective method to enhance the productivity of a still [13, 14]. The main reasons for the enhancement include acceleration of the vapor diffusion and reduction of non-condensable gas under vacuum condition. Two ways are usually employed to provide vacuum inside a solar still, i.e., using mechanical pumping [13] or natural vacuum [15]. Natural vacuum adopts the force of gravity. This method does not need mechanical pumping once in operation except for the initial start-up of the process [16]. Distillation efficiencies of 47.6% and 65% were reported for single [14] and double [17] effect solar stills with natural vacuum, respectively. The disadvantage of natural vacuum method is that the evaporation chamber needs to be

placed ~10 m higher above the saline water, which will extremely increase the construction difficulty and the cost of the desalination system. On the other hand, maintain vacuum with a vacuum pump is less demanding on the construction and the operating pressure can be easily adjusted. Ahmed et al. [18] tested a three-effect solar still coupled with a vacuum pump in an outdoor experiment. The daily freshwater yield reached 14.2 kg/m^2 with the operating pressure of 0.5 bar, which was 45% higher than that under atmospheric conditions. A tubular-type solar still has good pressure bearing performance, which has attracted widespread attention [19-21]. Zheng et al. [22] found that the yield rate of the tubular still increased from 0.71 kg/m^2/h to 1.9 kg/m^2/h when the operating pressure was reduced from 101 kPa to 20 kPa at a heating temperature of 60 °C. Our previous work quantitatively indicated the electricity consumption of the vacuum pump [23], where the pump requires a power supply of approximately 9 W to maintain 20 kPa inside a tubular solar still. The results also showed that the cumulative electricity consumption to produce 1 kg fresh water at 20 kPa and 62 °C was 0.033 kWh.

Apart from productivity enhancement, vacuum operation also lowers the evaporation temperature, which mitigates the fouling problem. However, an adverse effect of the lower evaporation temperature under vacuum operation is the low heat discharge from the outer surface to the ambient air, as the outer surface temperature is also lower than operating at normal pressure. This in turn hinders the vapor condensation process which eventually leads to vapor accumulating in the still [24]. In our previous experimental study, continuous suction of vapor by vacuum pump was observed when operating pressure was lower than 40 kPa. This phenomenon was caused by the poor cooling capability of the tubular solar still, and led to an unexpected decreasing efficiency. In this situation, many researchers dedicated to combining solar stills with cooling enhancement techniques, eliminating the possibility of vapor loss from the system. The main methods include external vapor condenser [14, 25], water [26] or air flowing [27] above the cover, thermoelectric cooling [28], etc. A recent study showed a 305% increase in productivity of solar still by jointly adopting vacuum operation and enhanced cooling method, where the temperature of the cooling water was 15 °C below the ambient temperature [29]. Bilgil and Hırlakoğlu [30] conducted experiments to investigate the distillation performance under 10–20 kPa at different condensation temperatures, and suggested that the temperature of 0 °C gave the best performance, as further decreasing the temperature leads to little improvement on productivity but significantly increases the energy consumption. The above-mentioned studies have proved the benefits of using an enhanced cooling method for vacuum-operated solar stills. However, most of these cooling techniques need additional electrical power to drive the cooling flow, and thereby increase the cost and complexity of the system.

In this study, we presented a novel multi-effect tubular solar still (TSS) integrated with immersion cooling. Immersing heat dissipation surface into bulk water is cheap and easy for cooling enhancement, which has been proven as an effective cooling method for solar panels [31] and electronic devices [32]. Meanwhile, vacuum condition

was applied in the still with a mini vacuum pump. The vacuum pump and the circulating pump in the present work were driven by a photovoltaic (PV) panel. In this way, the system is completely self-sustainable, and is thereby applicable for standalone operation in remote areas. An outdoor experiment was conducted to investigate the performance of the still. The distillation productivity with and without the immersion cooling was compared. A cost analysis was then undertaken to compare different alternative techniques for desalination systems.

2 Materials and methods

Experiments were conducted to characterize the performance of the vacuum-operated solar still with and without immersion cooling. Two desalination systems were built with nearly identical configurations. In one system, the TSS was immersed in stationary water to lower its surface temperature; while in the other one, the TSS was exposed to air and cooled by natural wind.

2.1 System description

A schematic representation of the desalination system is shown in Fig.1. The specifications of the various devices in the system are listed in Table 1. The system is composed of a three-effect TSS, an immersion tank, a 12-W water pump, a solar collector, a solar PV panel and an 8-W vacuum pump. In our previous attempt [33], a 120-W vacuum pump was used in the experimental system, while it was too cumbersome and costly for small-scale solar stills. The water pump circulates hot water between the solar collector and TSS. The vacuum pump connected to the cylindrical tanks is used to draw the air out of the TSS. Both pumps are powered by the PV panel. In operation, solar energy is harvested by the solar collector and heats the water stored in the collector. Saline water in the still is heated and vaporizes under vacuum condition. The vapor condenses on the inner shell surface in each effect. The distilled water trickles into the freshwater tank via an outlet tube at the bottom of the TSS. The 8-W vacuum pump is periodically operated every one hour for a few minutes to maintain a pre-set pressure inside the still. In contrast, either a fixed pressure was kept strictly with a pressure switch [34], or the pump was operated only once before the daylight [35], or a continuous-running vacuum fan was adopted [36].

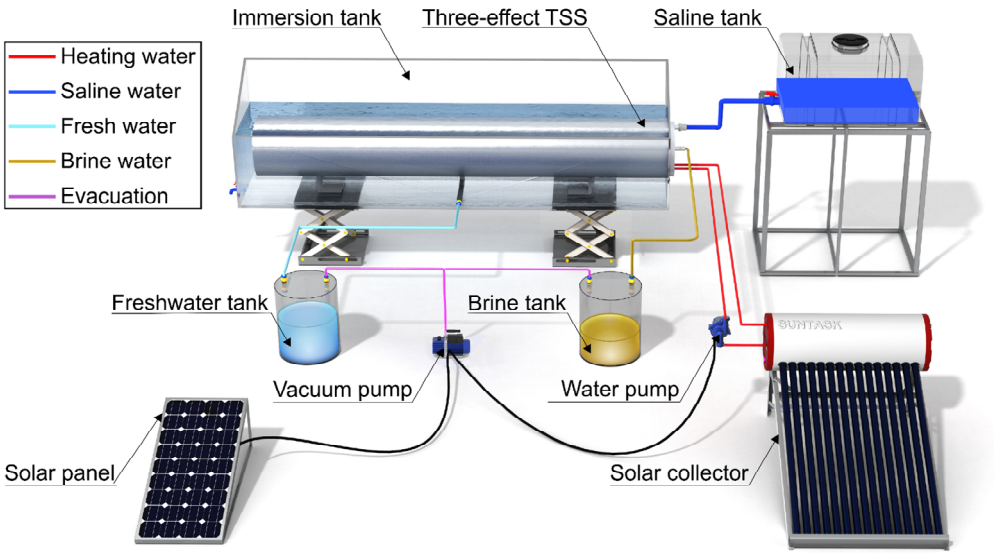

Fig.1. Schematic of the proposed solar distillation system with immersion cooling.

Table 1

Specifications of the devices of the distillation system.

Device	Specifications
Evacuated tube solar collector	Absorbing area = 1.09 m^2
Solar PV panel	Absorbing area = 0.19 m^2; output power = 30 W; maximum voltage= 17.8 V; maximum current = 1.69 A
Vacuum pump	Operating voltage = 12 V; power consumption = 8 W; flow rate = 8 L/min
Circulating water pump	Operating voltage = 12 V; power consumption = 10 W; flow rate = 2.2 L/min
Saline tank	Maximum water storage = 50 L
Freshwater tank	Maximum water storage = 10 L
Brine tank	Maximum water storage = 10 L

2.2 Design of the prototype

A compact three-effect TSS was adopted in this study and its structure is illustrated in Fig.2. The TSS has a nested structure which is commonly used for small-scale multi-effect distillation owing to the efficient heat recovery and low vapor diffusion resistance [37, 38]. The still is composed of three effects, denoted as effect #1, #2 and #3 from inside to outside, which is shown in Fig.2(a). Each effect consists of a pair of concentric shell and trough. Two cylindrical inner supports are symmetrically welded beneath the bottom of the shell to support the trough. Two pairs of pipes are welded in the endplates, i.e., saline pipes and freshwater pipes. The U-shaped saline pipes are designed for cascade fill of saline water. The straight freshwater pipes act as the transportation passages for freshwater, through which the freshwater produced in effects #2 and #3 is finally transferred to effect #3 and confluences into the freshwater tank. The

mechanisms of saline water filling, freshwater confluence and brine overflow were illustrated in Fig.2(b). The water capacities of troughs #1, #2 and #3 are approximately 6.6, 6.7 and 10.8 kg, respectively; the corresponding evaporation areas are 0.13, 0.17 and 0.18 m^2, respectively. The outmost shell is 1.6 m in length. The detailed specifications of the TSS can also be referred to in [33].

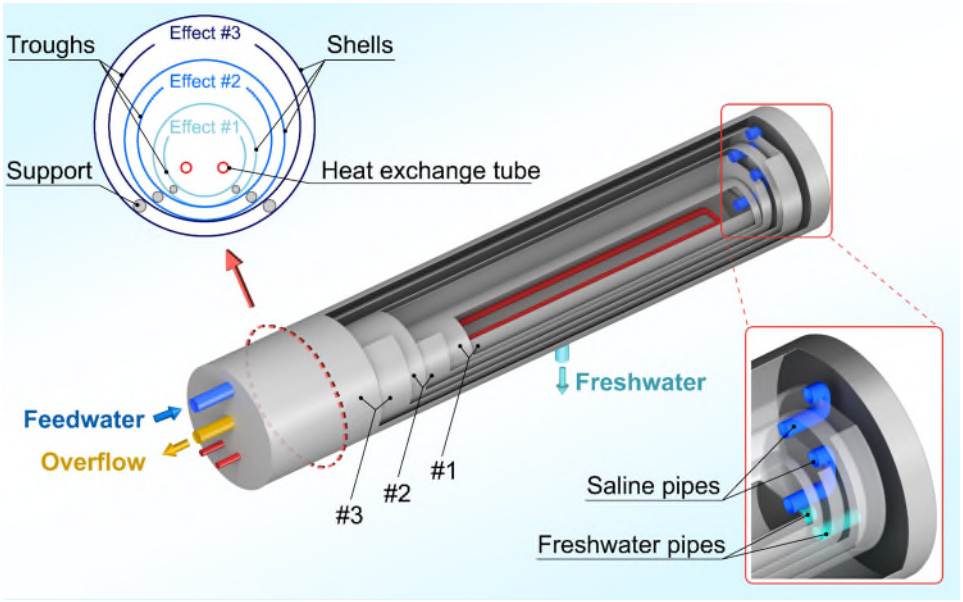

(a) Structure of three-effect TSS

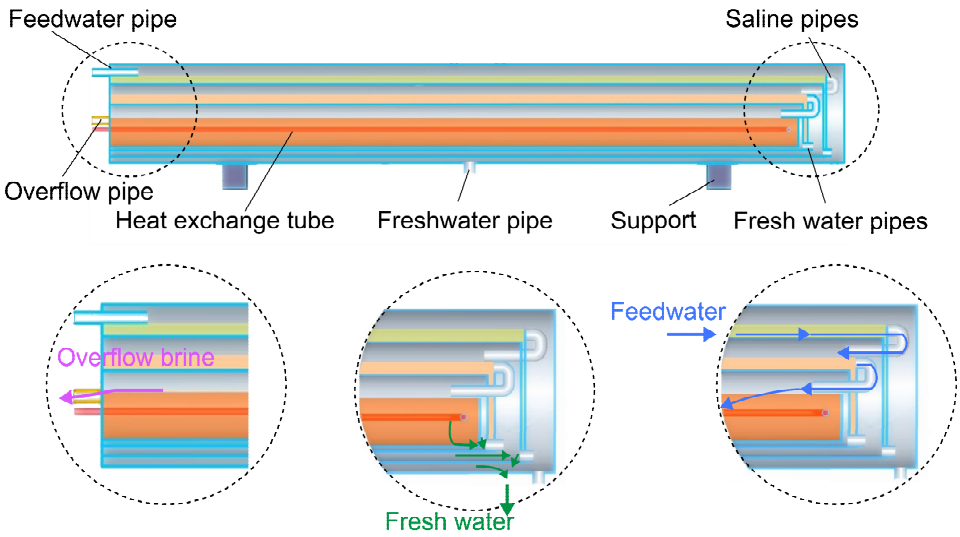

(b) Flow of feedwater and fresh water inside TSS

Fig.2. Structure diagram of the three effect TSS.

Before the operation, saline water is fed into the TSS from the saline tank by gravity. The feedwater is supplied to effect #3, #2 and #1 sequentially. Trough #3 is firstly filled up and the exceeded saline overflows into trough #2 through the U-shaped pipe. Similarly, the saline is fed into trough #1 after trough #2 is full. The excess saline for the still finally overflows through the pipe on the end plate and is collected by the brine tank. During the desalination process, saline water in effect #1 is heated by the circulating water and vaporizes at the operating pressure. The saline water in effects #2

and #3 was heated by the generated vapor from the previous effect. Generated vapor in the three effects condenses on the inner surface of the shell similarly. The condensate trickles into the freshwater tank via an outlet tube at the bottom of the TSS.

The vapor condensation within the still is enhanced by immersing the still into bulk cooling water, as schematically shown in Fig.3. The dimensions of the immersion tank are presented in the left of the figure. The tank is made of 10-mm thick Plexiglas plates. The maximum storage volume of the tank is 216 L. A circular opening was prepared in the right plate to accommodate the end plate of the TSS. A valve was installed on the left plate to drain the cooling water. A pipe on the bottom of the still was assigned to connect the freshwater outlet and the freshwater tank through an orifice in the front plate. Silicone sealants were used to seal all the openings and orifices of the tank. The sectional view on the right side of Fig.3 illustrates the cooling process of the shell immersed in water. The upper part of the shell absorbs latent heat of vapor condensation and the dissipation heat is then released to the cooling water mainly by convection. Preliminary tests indicated that the lower part of the shell absorbed hardly any heat from the vapor and its temperature was approximately equal to the cooling water temperature. The water is finally cooled by the surroundings. The vertical wall can partially block the wind flow and create a recirculation zone, thus enhancing the heat transfer between the wind and the cooling water [39].

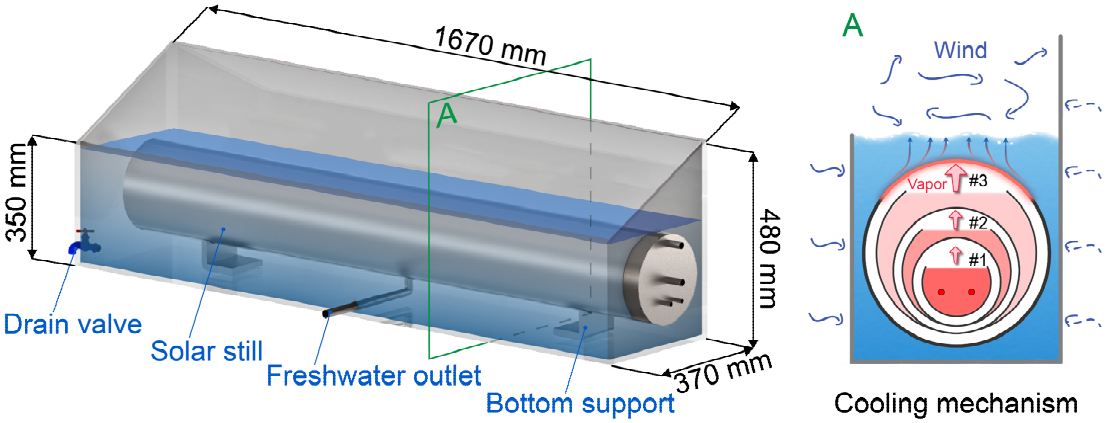

Fig.3. Schematic drawing of the immersion cooling.

2.3 Experimental setup

A field test with experimental system shown in Fig.4 was conducted in Xichang (27° 55′ N, 102° 17′ E), China. The atmospheric pressure at the test site was 91 kPa. Two groups of experiments were carried out during March 2019, using TSS with (see Fig.4(a)) and without (see Fig.4(b)) immersion cooling. The locations of the temperature sensors in different experiments were shown in Fig.4(c) and (d), respectively. The cooling water and the raw saline water were collected from the lake (Qionghai Lake) near the test site.

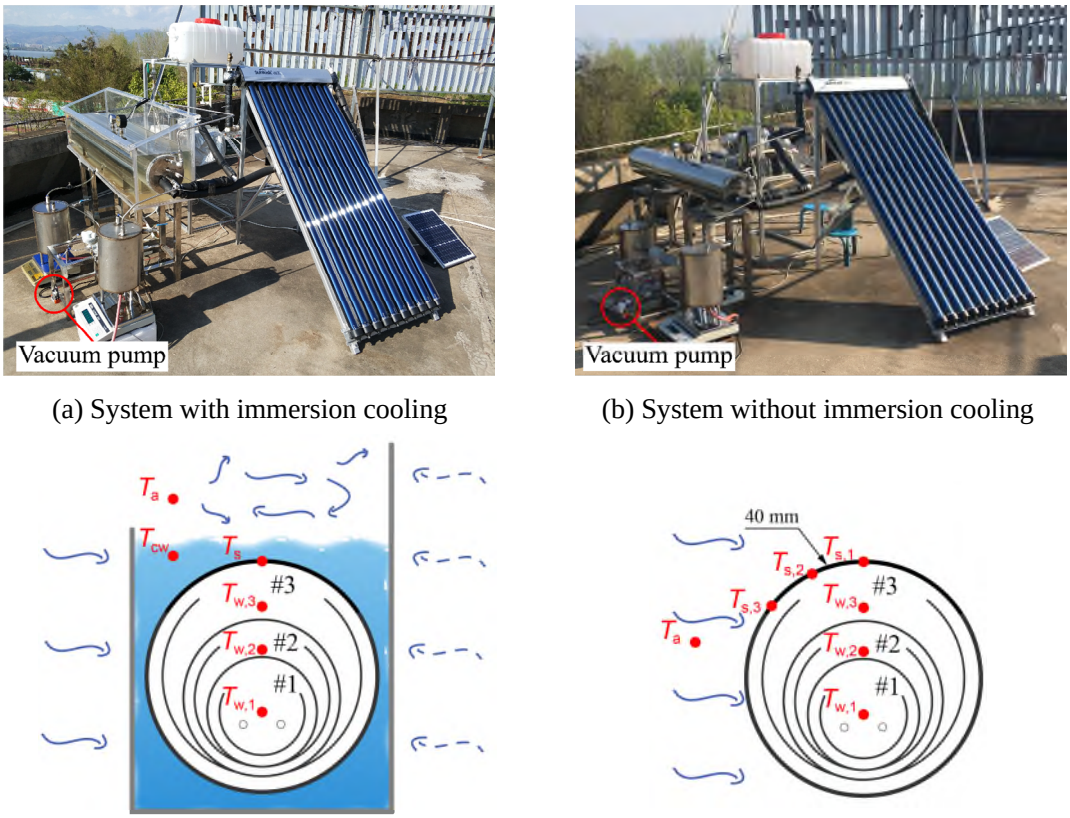

(a) System with immersion cooling (b) System without immersion cooling

(c) Sensor locations with immersion cooling (d) Sensor locations without immersion cooling

Fig.4. Experimental system and sensor locations.

The measuring instruments and their corresponding accuracy are listed in Table 2. The instantaneous solar intensity was measured with a pyranometer. The wind speed was monitored by a hot-wire probe. Data of the solar radiation and the wind speed were logged by a portable data logger at a one-minute interval. Thermocouples were used to measure the temperatures at different positions, including the ambient, the circulating water, the saline water in the three troughs, the top of the outer shell and the cooling water. For tests without immersion cooling, five resistance temperature detectors (RTD) were used to measure the temperature of the outer surface of the shell. In this case, RTDs were circumferentially fixed on the upper region of the outer tubular shell at 40 mm intervals. All the temperature data were acquired by a data recorder every one minute. The operating pressure inside the TSS was measured with a piezometer mounted on the top of the outer shell. The fresh water and the overflow brine were separately collected by two tanks and weighed by two electronic scales. The flow rate of the feedwater was measured with a float-type flow meter and adjusted with a needle valve. The electrical conductivity and total dissolved solids (TDS) of water were obtained with a digital meter.

Table 2

Accuracy for various measuring instruments.

Instrument	Range	Accuracy
Thermocouple	0–100 °C	±0.5 °C
RTD	0–100 °C	±0.35 °C

Scale	0–15 kg	±0.5 g
Piezometer	0–101 kPa	±1.6%
Pyranometer	0–2000 W/m^2	±3%
Pressure controller	0–101 kPa	±2.5%
Flow meter	2.04–98.4 mL/min	±2%
Hot-wire probe	0.05–40 m/s	±0.2 m/s
Data recorder	–	±0.2%
TDS meter	0–4999 ppm	±2%

Five tests were conducted on 20th (i), 25th (ii), 28th (iii), 29th (iv), 30th (v) of March in which month of the year the solar radiation in Xichang is the highest [40]. Cases (i), (ii) and (iii) correspond to the still with immersion cooling operated at 40, 60 and, 91 kPa (absolute pressure), respectively. Cases (iv) and (v) correspond to the still without immersion cooling operated at 40 and 60 kPa, respectively. Operating procedure for the tests is shown below:

1− Before the test, the saline was replenished in all the troughs of the still until all the troughs were filled up. The operating pressure was regulated to the desired pressure using the vacuum pump.

2− The start time of the hot water circulation pump was flexible depending on the solar irradiation, i.e., activated at the time when the solar radiation flux exceeded 200 W/m^2.

3− During the test, the vacuum pump was operated every one hour to maintain the pressure. The weight of the freshwater tank was recorded every 30 minutes. The circulating pump was turned off at 18:30 local time.

4− The fresh water was drained out from the collecting tank at 7:30 the next day. Its weight and quality were subsequently measured with instruments.

2.4 Uncertainty analysis

The reliability of the experimental results was obtained through an uncertainty analysis for the measured parameters as well as the distillation efficiency. The uncertainties were calculated following the “Kline and McClintock” method [41], i.e.,

$$u_c(y) = \sqrt{\sum_{i=1}^{n}\left(\frac{\partial y}{\partial x_i}\right)^2 u^2(x_i)} \quad (1)$$

where, $u_c(y)$ is the combined uncertainty, y is an experimental output value calculated from a set of measurements and is given by $y = f(x_1, x_2, \ldots, x_n)$, x_i is the individual measurement, and $u_c(x_i)$ is the uncertainty of x_i. The uncertainties of the measured and calculated data are listed in Table 3.

Table 3

Uncertainties of the measured and calculated quantities.

Quantities		Case (i)	Case (ii)	Case (iii)	Case (iv)	Case (v)
Daily Yield	Value (kg)	10.688	8.013	5.577	7.236	6.008

	Uncertainty (%)	±0.005	±0.006	±0.009	±0.007	±0.008
Average temperature	Value (°C)	66.9	68.3	64.4	72.7	70
	Uncertainty (%)	±0.95	±0.93	±0.98	±0.89	±0.91
Solar radiation flux	Value (W/m^2)	637.9	648	496	601.9	494.7
	Uncertainty (%)	±3	±3	±3	±3	±3
PR	Value	1.87	1.52	1.25	1.45	1.31
	Uncertainty (%)	±0.009	±0.01	±0.02	±0.02	±0.02
SEC	Value (kJ/kg)	5.21	1.73	0	3.65	1.36
	Uncertainty (%)	±0.013	±0.072	–	±0.042	±0.16

3 Results

3.1 Climatic conditions and pressure regulation

Solar radiation intensity has a significant effect on the productivity of a solar still since it determines the instantaneous input heat of the desalination system. A higher solar intensity brings a higher temperature of saline, which facilitates the evaporation process. The weather of the test day was sunny for case (i), (ii) and (iv), while it was cloudy for case (iii) and (v). The curves of solar radiation flux are almost smooth for sunny days, as shown in Fig.5. Significant fluctuations for case (iii) and (v) are observed in 10:00–13:00 and 12:00–15:00, respectively. The maximum fluxes are obtained at midday and the corresponding values are listed in Table 4 as well as other climatic data.

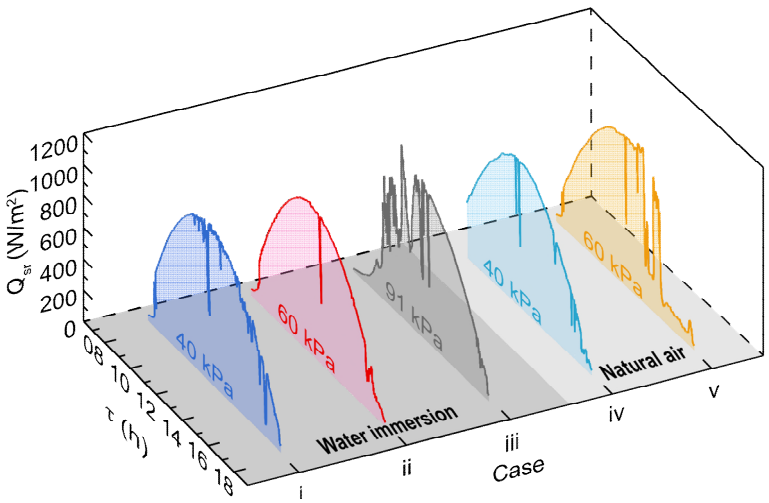

Fig.5. Variations of solar intensity for cases with different cooling methods.

Climatic conditions and cumulative solar radiation.

Case No.	Cooling method	P_{op} (kPa)	T_a (°C)	$Q_{sr,max}$ (W/m^2)	R_{sr} (MJ/m^2)	V (m/s)			
						8:30	12:00	18:00	Average
(i)	Water	40	21.7	976	24.1	0.264	1.556	0.336	0.72

(ii)	Water	60	22.1	922	22.2	0.792	0.734	1.01	0.85
(iii)	Water	91	16.9	1052	18.9	0.488	1.506	0.344	0.78
(iv)	Air	40	23.6	896	21.0	0.624	1.03	0.446	0.70
(v)	Air	60	23.4	939	19.4	0.418	1.262	0.432	0.71

The variation of P during the tests was shown in Fig.6. The pressure was well regulated by the 8-W vacuum pump for cases (i)&(ii) (see Fig.6(a)). In these two cases, the corresponding pressure stabilized around the pre-set value with minor fluctuation. A sharp rise of P at around 18:20 in case (i) was caused by turning on the valve in the freshwater tank to release fresh water, which had a negligible effect on the productivity since the solar radiation was extremely low in this period. A consecutive rise in P during 14:00–17:00 was observed for case (iv). This is due to the excessive vapor that cannot be condensed within the chamber. The low heat transfer from the surface to the ambient air hindered the condensation of the vapor. The vapor accumulation outcompeted the vacuum pumping, which led to increased pressure. In this situation, pressure regulation for the still did not work. Even worse, unnecessary evacuation of the distillation chamber led to massive vapor loss. To reduce the loss, the pump was shut off at 15:30. It can also be observed in case (iv) that P decayed after 17:00, which is due to the declined generated rate of vapor within the still. While for case (v), the pump was shut off at 15:00 due to the natural drop of pressure within the chamber. This natural drop of pressure arose from the more condensed vapor than generated vapor as solar radiation steeply dropped, i.e., reduced vapor in the chamber resulted in decreasing pressure.

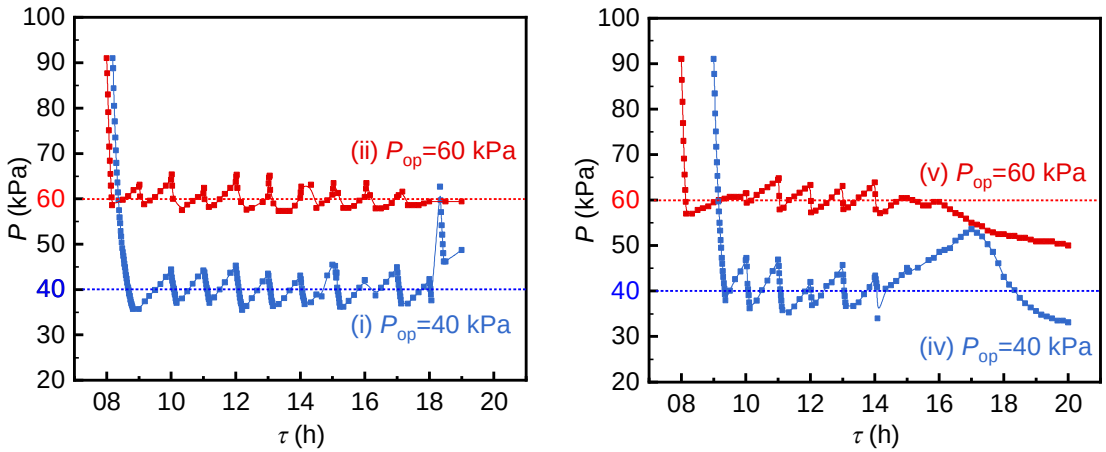

(a) Water immersion cooling (b) Natural air cooling

Fig.6. Pressure fluctuations in distillation chamber.

3.2 Temperature variations

The measured variations of the temperatures at different positions were present in Fig.7, showing the temperatures of the circulating heating water (T_h), the saline water ($T_{w,i}$), the outmost shell (T_s), the cooling water (T_{cw}) and the ambient (T_a). T_h increased rapidly before the circulating pump was turned on since the solar energy only heated the water stored in the solar collector. After turning on the circulating pump, the circulating water directly heated the saline in trough #1. The heat was then sequentially

transferred from the inner effect to the outer one mainly through the convection and condensation of vapor. T_w of each effect rose quickly in the first 2 hours. The exhaust heat was finally released to the cooling fluid through the outer shell for different cooling methods. For the tests of natural air cooling, T_s was higher than $T_{w,3}$ during 8:30–11:30 as can be seen in Fig.7 (d) and (e). This phenomenon deteriorated the productivity of TSS with natural air cooling since the vapor generated by effect #3 cannot condense on the shell at the beginning, and limits the vapor condensation in the following hours. However, this deterioration was greatly attenuated by immersing the shell in cooling fluid, contributing to a lower T_s during the yielding process (see in Fig.7 (a), (b) and (c)). During noon hours, T_s in cases with water immersion was lower than 35 °C, while for natural air cooling it was higher than 60 °C. The circulating pump was turned off at 18:30 when T_h is approximately lower than $T_{w,1}$. The oscillation in Fig.7(c) at around 17:00 is because of the occasional signal interference on the data recorder from the environment.

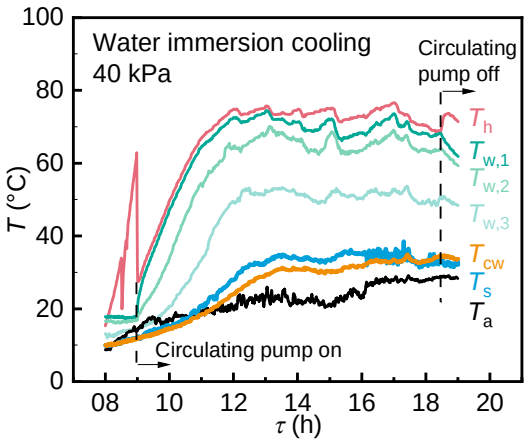

(a) Case i

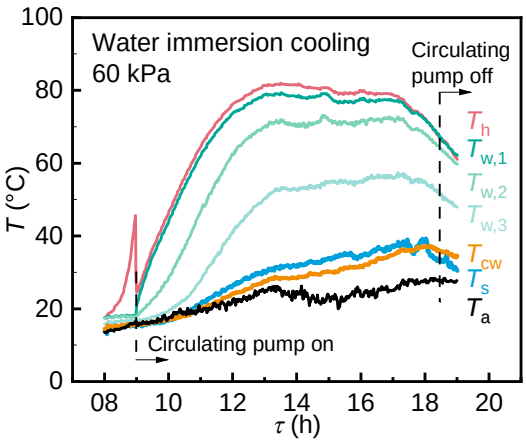

(b) Case ii

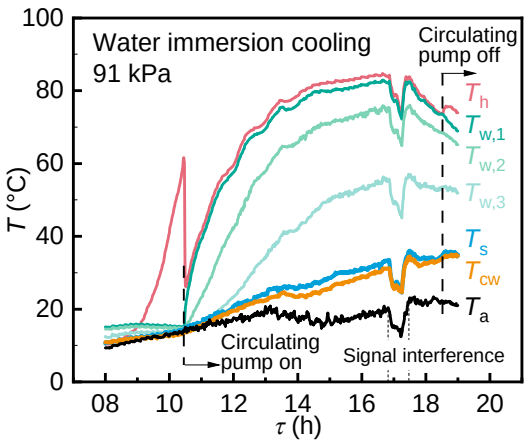

(c) Case iii

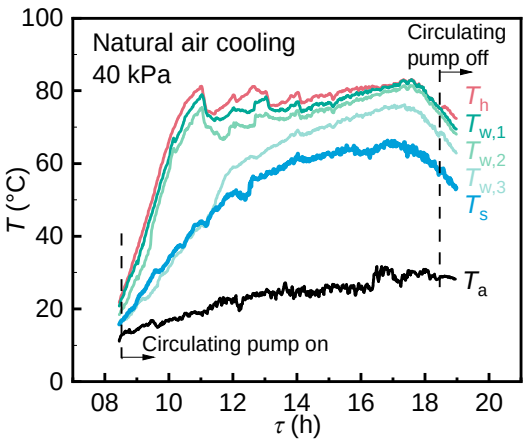

(d) Case iv

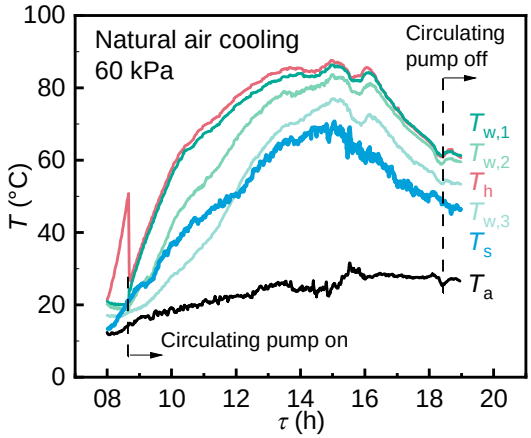

(e) Case v

Fig.7. Variations of the temperatures during the tests.

The operating temperature of the still is also affected by operating pressure, which is indicated in Table 5. The data generally represents a declining trend in operating temperature with decreasing operating pressure, even for the cases with very different solar radiations.

Table 5

The maximum temperature at different positions.

Case No.	P_{op} (kPa)	$T_{w,1}$ (°C)	$T_{w,2}$ (°C)	$T_{w,3}$ (°C)	T_s (°C)
(i)	40	74.5	70.1	53.7	38.5
(ii)	60	79.4	73.1	57.4	39.3
(iii)	91	82.9	76	57.1	36
(iv)	40	83.1	81.5	76.2	66.3
(v)	60	86.4	83.7	77	70.7

3.3 Freshwater yield rate

The freshwater yield was measured every 30 minutes and the yield rate was shown in Fig.8. The yield rate increased gradually after the circulating pump was switched on. It reached a relatively steady value (1.4 kg/h) during 12:30–17:30 for case (i), while the steady $\dot{m}$ were 1.1 kg/h for case (ii) and 1.0 kg/h for case (iii).

As shown in Fig.8(a), the required time to reach the maximum $\dot{m}$ in cases (i), (ii) and (iii) were approximately 3, 5 and 7 h, respectively, showing that more time was needed for cases of higher P_{op}. One reason can be attributed to the higher proportion of non-condensable gas in the distillation chamber at higher P_{op}, which leads to the deterioration of the heat transfer process. Besides, the mass transfer process under lower operating pressure will be enhanced, resulting in faster vapor diffusion and shorter transportation time. The maximum $\dot{m}$ in cases (i), (ii) and (iii) were approximately 1.5, 1.5 and 1.1 kg/h, but note that maximum $\dot{m}$ of cases (ii) at 16:00 was possibly interfered by retaining freshwater in the earlier period and the actual value should be smaller than 1.5 kg/h.

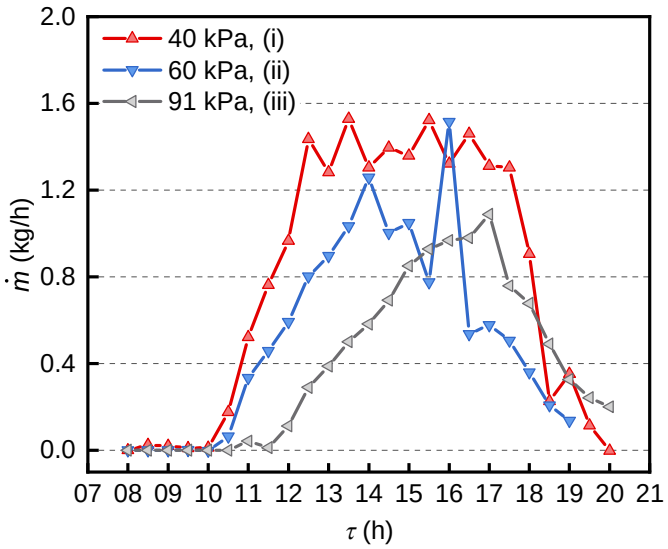

(a) Water immersion cooling

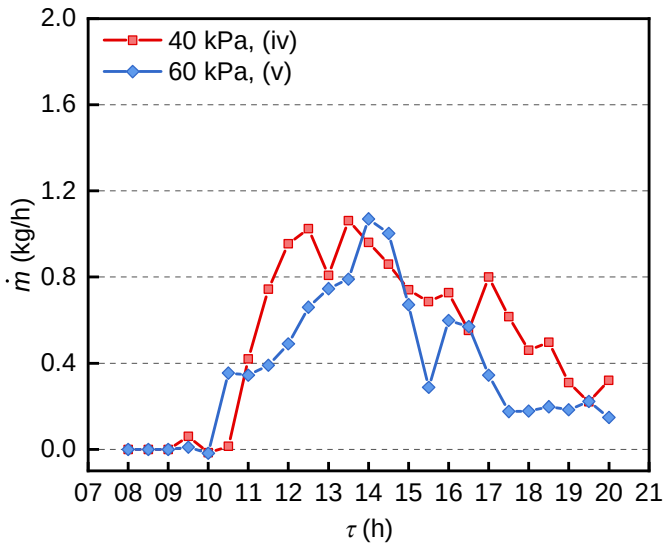

(b) Natural air cooling

Fig.8. Freshwater yield rate during the tests.

The total production of the still is increased with the reduced operating pressure, as listed in Table 6. The data in our previous study with natural air cooling at atmospheric pressure was also presented here as case (vi) [33]. The accumulated solar radiation for case (vi) is 16.8 MJ/m^2, and the average wind velocity is 0.8 m/s, closely resembling V_{avg} of cases (iv) and (v). For cases with water immersion cooling, the total production at P_{op} = 40 kPa was 33% and 92% more than that at 60 and 91 kPa, respectively. A similar result was observed in the cases with natural air cooling, where the total production at P_{op} = 40 kPa was 20% and 120% more than that at 60 kPa and 95 kPa. However, the electricity demand was also increased for cases with lower operation pressures due to the extended operation time of the vacuum pump. Nevertheless, immersion cooling could significantly enhance productivity and be practicable for a solar still operating under vacuum. The electricity consumptions in different cases will be discussed in subsection 4.3. The highest daily freshwater yield was found to be

10.688 kg, which was 48% higher than that with air cooling at the same P_{op}. A proportion of freshwater (24% at most, at P_{op} = 60 kPa) was produced during nighttime due to the sensible heat stored in the saline water. A water sample was also analyzed before and after the distillation process in terms of TDS and electrical conductivity (shown in Table 7). The TDS of the water was reduced from 126 mg/L to 4 mg/L after desalination.

Table 6

Day and nocturnal productivity of the TSS under different operating conditions.

Case No.	Cooling method	Pressure (kPa)	Daytime yield (kg)	Nocturnal yield (kg)	Total (kg)
(i)	Water	40	9.656	1.032	10.688
(ii)	Water	60	6.053	1.96	8.013
(iii)	Water	91	5.063	0.514	5.577
(iv)	Air	40	6.41	0.826	7.236
(v)	Air	60	4.708	1.3	6.008
(vi)[33]	Air	95	2.954	0.316	3.27

Table 7

Characteristics of product water.

	TDS (mg/L)	Electrical conductivity (μS/cm)
Feed water	126	252
Production	4	9

3.4 Cooling capacity of water immersion method

The cooling capacities of the two cooling methods are compared by calculating the overall heat transfer coefficient h_{sa} (details are provided in Appendix A), as shown in Fig.9. Radiant heat transfer was neglected in the calculation for cases with water immersion cooling since the radiant heat transfer coefficient (h_{rad}) is estimated to be less than 2% of the convective heat transfer coefficient (h_{con}). Fig.9(a) presents h_{sa} and the T_s during the tests of P_{op} = 40 kPa. When the solar still was immersed into the bulk water, $h_{sa,water}$ was approximately 15–50 times larger than $h_{sa,air}$. The maximum values of $h_{sa,water}$ and $h_{sa,air}$ were 445.6 and 8.7 W/(m^2·K), respectively. The average values of $T_{s,water}$ was 28.8 °C, which is nearly 25 °C lower than $T_{s,water}$ owing to the higher heat transfer coefficient of water cooling. Meanwhile, the immersed outer shell was kept cool after 13:00 due to the heat capacity of the cooling water, whereas $T_{s,air}$ gradually increased. As shown in Fig.9(b), The relative magnitude of $h_{sa,water}$ versus $h_{sa,air}$ for the cases at 60 kPa is similar with that at 40 kPa. T_s significantly dropped after 15:00, which is stemmed from the abrupt reduction of the solar radiation.

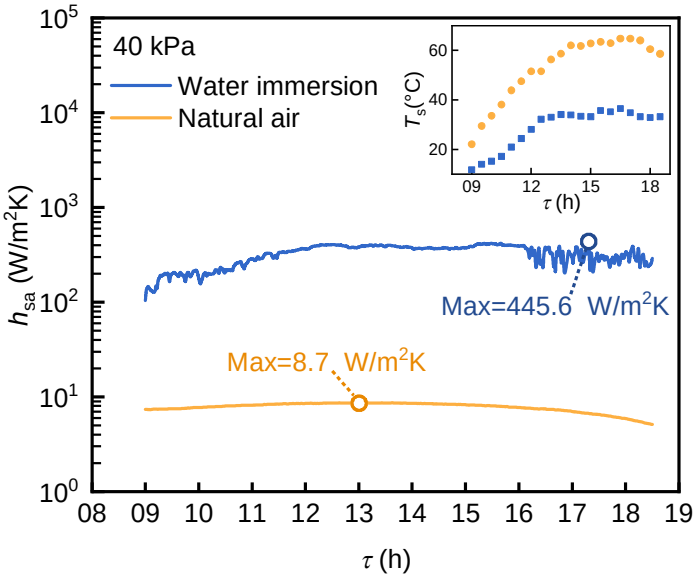

(a)

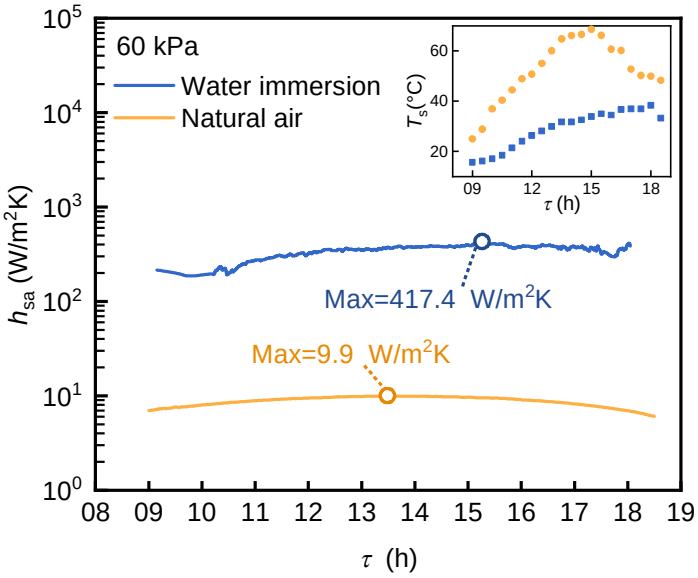

(b)

Fig.9. Cooling heat transfer coefficient and shell temperature at (a) P_{op} = 40 kPa and (b) P_{op} = 60 kPa.

4 Discussion

4.1 Performance ratio

Performance ratio (*PR*) is an important index to indicate the distillation efficiency of a still and commonly defined by Eq.(1):

$$PR = \frac{M_t h_{fg}}{E_s} = \frac{M_t h_{fg}}{A_{sc} R_{sr} \eta_c} \quad (2)$$

where M_t is the total freshwater yield, E_s is the total heat energy input to the still, h_{fg} is the latent heat of evaporation, A_{sc} and η_c are the surface area and the thermal efficiency of the solar collector, respectively. The collector is manufactured by Suntask® (model: SCM01), and its average daily efficiency is taken as 0.5 [42]. The values of *PR* with two different cooling methods are compared in Fig.10, including the result in our previous experiment conducted at 95 kPa with natural air cooling. *PR* of the still with immersion cooling was significantly elevated under various operating pressures. The highest *PR* was 1.87 at 40 kPa with water immersion cooling, i.e., a 187% thermal efficiency was realized by repeated energy utilization.

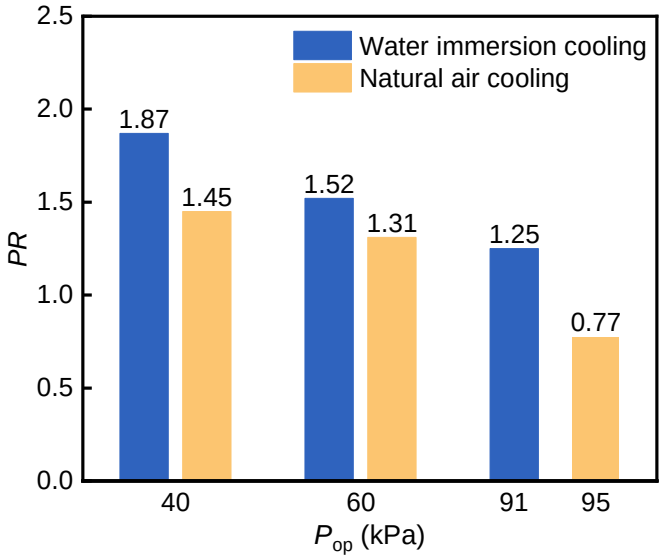

Fig.10. *PR* of the solar still with different cooling methods.

4.2 Cost analysis

The cost analysis is of great concern for solar desalination system, commonly used to evaluate economic performance. The initial investment of the system is listed in Table 8 based on local prices of the components, which is approximately $415 in total. A timer relay is applied to control the vacuum pump periodically. The procedure described in [43, 44] was followed to calculate the cost per liter (*CPL*) of distilled water. The interest rate, the life and the average operation time of the system are considered as 0.05, 20 years and 270 days per year, respectively. The average daily yield of fresh water is taken as 10.7 kg according to the experimental data of case (i). The *CPL* of the present desalination system with water immersion cooling and P_{op}=40 kPa is estimated to be $0.012.

Table 8

Initial investment for the present solar desalination system.

Components	Cost ($)

Three-effect tubular solar still	80
Evacuated tube solar collector	120
Circulating water pump	15
Vacuum pump	10
Timer relay	5
Photovoltaic module	30
Feedwater tank and frame	30
Brine and distillate tanks	30
Valves	10
Connecting pipe	5
Immersion tank	80
Total	415

The adoption of auxiliary equipment, including the vacuum pump, the timer relay and the immersion tank, enhances productivity but meanwhile increases the initial investment. Previous study indicated that the cost of water production can achieve at least a 20% decrease with vacuum operation [45] or multi-effect arrangement [46]. The *CPL* of the present system in different configurations were calculated, and compared with other similar systems, as shown in Table 9. In cases of different configurations, the *CPL* of water immersion was 20% lower than that of air cooling. The *CPL* was significantly decreased from 0.023 to 0.012 via vacuum operation, which makes the proposed technique more affordable for residents.

Table 9

Comparison of freshwater cost among different desalination systems.

Type	Description	Productivity (L/d)	*CPL* ($/L)
Three-effect still (present)	P_{op}=40 kPa, water immersion cooling	10.7	0.012
	P_{op}=40 kPa, natural air cooling	7.2	0.015
	P_{op}=91 kPa (no vacuum pump), water immersion cooling	5.6	0.023
Single-effect still [47]	Conventional type	3.9	0.035
Single-effect still [48]	With PCM tubes	0.45	0.008
Single-effect still [49]	Hemispherical still with copper tray	0.74	0.009
Single-effect still [36]	Vacuum fan, nanoparticles	9	0.035
Three-effect still [33]	With solar collector	5	0.012
Four-effect still [50]	Water cooling from top surface	27.1	0.013

4.3 Pressure control and electricity consumption

Vacuum operation enhances the productivity of solar stills by reducing boiling temperature and removing non-condensable gas [22, 51]. The operating pressure in the solar still was adjusted using a vacuum pump. The pump was switched on during the start-up period until the pressure reached P_{op}, and then was operated manually at an

interval of one hour to maintain the average pressure at P_{op}. The specific electricity consumption (SEC) per unit of produced water by the vacuum pump is defined as Eq.(2).

$$SEC = \frac{E_{vc}}{M_t} \tag{3}$$

where E_{vc} is the total electricity consumption of the vacuum pump during the test period including start-up. SEC was used to evaluate and compare the pressure control scheme for various vacuum-operated solar stills, though the demanded electricity in the proposed system was completely produced by solar energy via the PV panel.

To further compare the present setup with previous desalination systems, values of SEC from the present and previous studies are presented in Table 10. The electricity consumption of the present system was much lower than that of the previous vacuum-operated systems, proving that a mini vacuum pump coupled with the periodic operation is cost-effective for small-scale solar stills. For the present system, SEC of air cooling was found to be smaller than that of water cooling. This is mainly because the pump was shut off earlier during the tests of air-cooling cases. The effect of more electricity consumption with longer pump operation of water-cooling case on SEC outcompetes the effect of more freshwater yield. Along with the increase in freshwater yield, SEC was remarkably increased as P_{op} reduced from 60 to 40 kPa. This trade-off between productivity and electricity consumption of vacuum operation should be considered in practical application.

Table 10

Comparison of distillation efficiency and electricity consumption for vacuum operation between different solar desalination systems.

Type	Vacuum device	Operating scheme	Pressure (kPa)	*PR*	Electricity consumption (kJ/kg)
Three-effect tubular (present)	8-W vacuum pump	Operation periodically at the interval of one hour	60	1.52	1.7 (water cooling)
			40	1.87	5.2 (water cooling)
			60	1.31	1.4 (air cooling)
			40	1.45	3.7 (air cooling)
Two-effect tubular [23]	120-W vacuum pump	Automatic operation at the accuracy of ±0.5 kPa	60	0.70	21.6
			20	1.1	345.4
Single-effect basin [25]	11-W vacuum fan	Continuous or intermittent operation	N/A	N/A	46.1
Single-effect basin [52]	550-W vacuum pump	Evacuating 5 mins during start-up period	15–55	0.17	366.7
Natural vacuum [14]	245-W vacuum pump	Evacuating 17 mins during start-up period	23	0.48	60.9

N/A: Not available.

4.4 Mechanism of productivity improvement due to immersion cooling

The immersion cooling generally lowered the operating temperatures in each effect of the still, changing the temperature difference between evaporation and condensation

surfaces (ΔT). The temperature difference has a significant impact on the productivity of solar stills [53, 54], which acts as a driving force for the distillation process. ΔT in each effect as well as the freshwater yields under both water and air cooling at P_{op}=40 kPa are presented in Table 11. ΔT_1 tended to decrease with time during the tests for both water- and air-cooling conditions. ΔT_2 increased first and then decreased from 09:00 to 14:00, and became relatively stable after 14:00. ΔT_3 was mostly affected by the cooling methods. Under the air-cooling condition, ΔT_3 tended to increase during the test, while with water cooling, ΔT_3 fluctuated before 14:00 and then stabilized. The average ΔT of effect #1, #2 and #3 were 6.5, 14.3 and 15.2 °C under water cooling condition, and the values under air cooling condition were 2.9, 11.3 and 5.6 °C. The average $\dot{m}$ was therefore higher under larger temperature differences, which benefited from better cooling performance of water against natural air.

Table 11

Comparison of ΔT in each effect and freshwater yield rate under water- and air-cooling conditions.

Local time (h)	$\Delta T_{1,avg}$ (°C)		$\Delta T_{2,avg}$ (°C)		$\Delta T_{3,avg}$ (°C)		$\dot{m}$ (kg/h)	
	Air	Water	Air	Water	Air	Water	Air	Water
09–10	4.9	10.1	16.4	8.1	-2.7	3.1	0.03	0.02
10–11	3.5	11.2	30.4	18.2	-1.4	9.2	0.00	0.09
11–12	4.4	8.7	18.8	17.2	3.0	18.3	0.58	0.64
12–13	4.2	6.7	10.2	14.3	7.6	20.2	0.99	1.20
13–14	2.6	4.1	7.0	15.3	6.9	18.5	0.94	1.41
14–15	1.9	5.4	4.9	14.2	7.4	16.8	0.91	1.35
15–16	1.7	3.9	4.4	13.0	8.5	16.4	0.71	1.44
16–17	1.4	4.5	4.4	14.2	10.3	17.2	0.64	1.39
17–18	1.5	4.3	5.5	14.4	11.0	17.3	0.71	1.31
Average	2.9	6.5	11.3	14.3	5.6	15.2	0.61	0.98

To further understand the enhancement mechanism of water immersion cooling, a theoretical analysis of freshwater productivity under different immersion temperature T_{cw} was conducted based on the model developed in [55]. The fresh water yielded from each effect were calculated under the condition of water cooling with T_{cw} in 5–50 °C and air cooling at T_a=20 °C (V=1 m/s), respectively. Solar radiation of case (ii) was adopted in this calculation, where P_{op} was set as 60 kPa. The results are presented in Fig.11. Compared with air cooling, the total yield is increased in cases of water immersion cooling, resulting from the increased yield from every effect. Nevertheless, the yield of effect #3 is decreased when T_{cw} is lower than 15 °C. Excessive cooling resulted from extremely low T_{cw} reduces the evaporation temperature of saline water in effect #3, and thus leads to less yield. In addition, we found the yield of single effect first rises and then falls with T_{cw} for all effects, wherein yield of effect #3 is the most sensitive one. This indicates that T_{cw} is needed to be considered for maximizing the overall productivity of a multi-effect solar still. Although water cooling can benefit the productivity, excessively low water temperature will decrease the operating temperature of the still, resulting in a low thermal efficiency [56]. In this case, the

optimum T_{cw} is approximately 40 °C, and low-temperature geothermal water is a selectable cooling source [29].

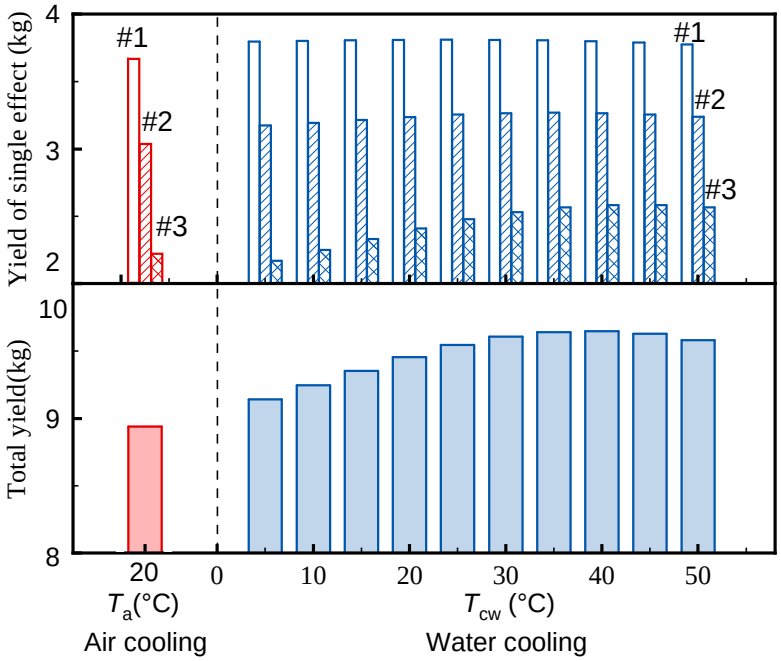

Fig.11. Theoretical yield of each effect and the total yield.

5 Conclusion

An innovative self-sustainable solar desalination system featured with water immersion cooling and vacuum operation has been proposed in this study. The system consists of a three-effect TSS, a solar collector, a cooling tank and a vacuum pump. A novel pressure control scheme for solar still was implemented and significantly reduced electricity consumption. The only external electricity required by the system is supplied by a 0.19-m^2 PV panel. A 5-day outdoor experiment was conducted and the overall performance of the system including freshwater productivity, efficiency, and electricity consumption were evaluated.

The experimental results reviewed a great improvement on existing desalination technique, including a significant daily freshwater yield of 9.8 kg/m^2/d achieved at P_{op} = 40 kPa, a maximum daily performance ratio of 1.87 and an extremely low forecast cost of $0.012/L for the distilled water. With the aid of the pressure control scheme, the electricity consumption had been lowered to 5.2 and 1.7 kJ/kg for 40 and 60 kPa, respectively. This demonstrated that periodic pressure regulation together with the use of a mini-vacuum pump can efficiently perform the vacuum operation of a small-scale solar desalination unit.

A comparison of the cooling heat transfer coefficients of water immersion cooling and natural air cooling suggests an overwhelming performance of former cooling method. The temperature of the outmost shell with water cooling was approximately

30 °C lower than that with air cooling, contributing to a higher freshwater yield under water-cooling condition. A theoretical analysis for cases of P_{op}=60 kPa indicated that excessively low water temperature will result in a low thermal efficiency and productivity of solar still. In this case, the optimum temperature of cooling water was approximately 40 °C.

The proposed self-sustainable solar desalination system addressed the defects of high electricity consumption and cooling insufficiency. The overall excellent performance of the proposed system supports the feasibility of a practical application. Yet, the long-term performance remains to be assessed, which is of interest in our further work in the next step.

Acknowledgments

We gratefully acknowledge the financial support for this research provided by National Natural Science Foundation of China (51606130).

Appendix A

The theoretical formulations of h_{sa}, h_{rad} and h_{con} are given below in details.

A.1 h_{sa}

The overall heat transfer coefficient from the outer shell to the ambient is defined as follows:

$$h_{sa} = h_{rad} + h_{con} = \frac{Q_d}{A_c \Delta T} \tag{A.1}$$

where h_{rad} and h_{con} are radiant and convective heat transfer coefficients, respectively; A_c is the heat transfer area and ΔT is the temperature difference between the outer shell and the cooling fluid; Q_d is the dissipated heat released to the environment by radiation and convection.

A.2 h_{rad}

Assuming a uniform temperature of the outer shell, h_{rad} can be calculated according to Eq.(A.2) [57]:

$$h_{rad} = \sigma \varepsilon_{ss} [\frac{(T_s + 273)^4 - (T_{sur} + 273)^4}{(T_s - T_c)}] \tag{A.2}$$

where T_s, T_{sur} and T_c are the temperatures of the outer shell, the surroundings, and the cooling fluid, respectively.

A.3 h_{con}

The convective heat transfer coefficient (h_{con}) is calculated as follows:

$$h_{con} = \frac{\lambda \overline{Nu}}{l} \tag{A.3}$$

where λ is thermal conductivity and l is the characteristic length.

A.3.1 Natural convection of immersion cooling

Natural convection occurs on the immersed outer shell. The average Nusselt number $\overline{Nu}$ over the shell can be calculated according to Eq.(A.4) [58]:

$$\overline{Nu} = 0.54 Ra^{0.25} \tag{A.4}$$

where Ra is Rayleigh number. Eq.(A.1) has been validated to estimate natural convection heat transfer for $10^4 < Ra < 10^7$, which is applicable for the current cases. Thermophysical properties of water were calculated by equations in [59].

A.3.2 Forced convection of air cooling

The $\overline{Nu}$ of crossflow forced convection from cylinders in air is calculated based on Eq.(A.5) [60]:

$$\overline{Nu} = 0.148 Re^{0.633} \tag{A.5}$$

where Re is Reynolds number.

Nomenclature

A_{sc}	collecting area of solar collector, m^2
E_s	total heat energy input into the still, kJ
h_{con}	convective heat transfer coefficient, $W/(m^2 \cdot K)$
h_{fg}	latent heat of evaporation, kJ/kg
h_{rad}	radiative heat transfer coefficient, $W/(m^2 \cdot K)$
h_{sa}	overall heat transfer coefficient on the shell, $W/(m^2 \cdot K)$
l	characteristic length, m
M_t	total freshwater yield, kg
$\dot{m}$	freshwater yield rate, kg/h
$\overline{Nu}$	average Nusselt number
P	pressure, kPa
P_{op}	operating pressure, kPa
PR	performance ratio
Q_d	dissipation heat transfer rate, W
Q_{sr}	solar radiation flux, W/m^2
Ra	Rayleigh number
Re	Reynolds number
R_{sr}	cumulative solar radiation, MJ/m^2
SEC	specific electricity consumption, kJ/kg
T_a	ambient temperature, °C
T_c	temperature of cooling fluid, °C

T_{cw}	temperature of cooling water, °C
T_h	temperature of heating water, °C
T_s	temperature of outmost shell, °C
T_{sur}	temperature of surroundings, °C
$T_{w,i}$	temperature of saline water, °C
u	uncertainty
u_c	combined uncertainty
V	wind velocity, m/s
V_{avg}	average wind velocity, m/s

Greek symbols

ΔT	temperature difference between evaporation and condensation surfaces, °C
ε_{ss}	emissivity of stainless steel
η_{sc}	efficiency of solar collector
λ	thermal conductivity, W/(m·K)
σ	Stefan–Boltzmann constant, W/(m^2·K^4)
τ	local time, h

Subscripts

a	ambient
avg	average
c	cooling fluid
con	convective
cw	cooling water
d	dissipation heat
h	heating water
i	number of the effect
op	operating
s	outmost shell of the still
sc	solar collector
sr	solar radiation
ss	stainless still
sur	surroundings
w	saline water
1	effect #1
2	effect #2
3	effect #3

References

[1] J. Alcamo, T. Henrichs, T. Rösch, World water in 2025: Global modeling and scenario analysis for the world commission on water for the 21st century, Kassel World Water Series, 2000; 2.
[2] G. Gude, Energy storage for desalination processes powered by renewable energy and waste heat sources, Appl. Energy 137 (2015) 877-898.
[3] V.P. Katekar, S.S. Deshmukh, Techno-economic review of solar distillation systems: A closer look at the recent developments for commercialisation, J Clean Prod 294 (2021) 126289.
[4] D.B. Singh, G.N. Tiwari, Exergoeconomic, enviroeconomic and productivity analyses of basin type solar stills by incorporating N identical PVT compound parabolic concentrator collectors: A comparative study, Energy Convers. Manage. 135 (2017) 129-147.
[5] A.M. Manokar, D.P. Winston, J.D. Mondol, R. Sathyamurthy, E. Kabeel, H. Panchal, Comparative study of an inclined solar panel basin solar still in passive and active mode, Sol. Energy 169 (2018) 206-216.
[6] M. Elashmawy, An experimental investigation of a parabolic concentrator solar tracking system integrated with a tubular solar still, Desalination 411 (2017) 1-8.
[7] M. Elashmawy, Effect of surface cooling and tube thickness on the performance of a high temperature standalone tubular solar still, Appl. Therm. Eng. 156 (2019) 276-286.
[8] M. Elashmawy, Improving the performance of a parabolic concentrator solar tracking-tubular solar still (PCST-TSS) using gravel as a sensible heat storage material, Desalination 473 (2020) 114182.
[9] S. Rashidi, M. Bovand, N. Rahbar, J.A. Esfahani, Steps optimization and productivity enhancement in a nanofluid cascade solar still, Renew. Energy 118 (2018) 536-545.
[10] A.K. Singh, R.K. Yadav, D. Mishra, R. Prasad, L.K. Gupta, P. Kumar, Active solar distillation technology: A wide overview, Desalination 493 (2020) 114652.
[11] L. Zhu, M. Gao, C.K.N. Peh, G.W. Ho, Recent progress in solar-driven interfacial water evaporation: Advanced designs and applications, Nano Energy 57 (2019) 507-518.
[12] G. Peng, S. Sharshir, Y. Wang, M. An, A. Kabeel, J. Zang, L. Zhang, N. Yang, Micro/nanomaterials for improving solar still and solar evaporation-A review, arXiv preprint:1906.08461 (2019).
[13] I. Altarawneh, M. Batiha, S. Rawadieh, M. Alnaief, M. Tarawneh, Solar desalination under concentrated solar flux and reduced pressure conditions, Sol. Energy 206 (2020) 983-996.
[14] M. Abbaspour, M. Faegh, M. Shafii, Experimental examination of a natural vacuum desalination system integrated with evacuated tube collectors, Desalination 467 (2019) 79-85.
[15] A. Rashid, T. Ayhan, A. Abbas, Natural vacuum distillation for seawater desalination – A review, Desalination and Water Treatment 57 (2016) 26943-26953.
[16] S. Al-Kharabsheh, D.Y. Goswami, Experimental study of an innovative solar water desalination system utilizing a passive vacuum technique, Sol. Energy 75 (2003) 395-401.
[17] V. Gude, N. Nirmalakhandan, S. Deng, A. Maganti, Feasibility study of a new two-stage low temperature desalination process, Energy Convers. Manage. 56 (2012) 192-198.
[18] M.I. Ahmed, M. Hrairi, A.F. Ismail, On the characteristics of multistage evacuated solar distillation, Renew. Energy 34 (2009) 1471-1478.
[19] S.W. Sharshir, Y.M. Ellakany, A.M. Algazzar, A.H. Elsheikh, M.R. Elkadeem, E.M.A. Edreis, A.S. Waly, R. Sathyamurthy, H. Panchal, M.S. Elashry, A mini review of techniques used to improve the tubular solar still performance for solar water desalination, Process Saf. Environ. Prot. 124 (2019) 204-212.

[20] H. Panchal, K.K. Sadasivuni, M. Israr, N. Thakar, Various techniques to enhance distillate output of tubular solar still: A review, Groundwater Sustain. Dev. 9 (2019) 100268.
[21] I. Mohan, S. Yadav, H. Panchal, S. Brahmbhatt, A review on solar still: a simple desalination technology to obtain potable water, Int. J. Ambient Energy 40 (2017) 335-342.
[22] H. Zheng, Z. Chang, Z. Chen, G. Xie, H. Wang, Experimental investigation and performance analysis on a group of multi-effect tubular solar desalination devices, Desalination 311 (2013) 62-68.
[23] T. Yan, G. Xie, L. Sun, M. Du, H. Liu, Experimental investigation on a two-effect tubular solar still operating under vacuum conditions, Desalination 468 (2019) 114057.
[24] G. Xie, L. Sun, Z. Mo, H. Liu, M. Du, Conceptual design and experimental investigation involving a modular desalination system composed of arrayed tubular solar stills, Appl. Energy 179 (2016) 972-984.
[25] E. Kabeel, Z. Omara, F.A. Essa, Enhancement of modified solar still integrated with external condenser using nanofluids: An experimental approach, Energy Convers. Manage. 78 (2014) 493-498.
[26] Y.A.F. El-Samadony, E. Kabeel, Theoretical estimation of the optimum glass cover water film cooling parameters combinations of a stepped solar still, Energy 68 (2014) 744-750.
[27] T. Arunkumar, R. Jayaprakash, A. Ahsan, D. Denkenberger, S. Okundamiya, Effect of water and air flow on concentric tubular solar water desalting system, Appl. Energy 103 (2013) 109-115.
[28] N. Rahbar, J.A. Esfahani, A. Asadi, An experimental investigation on productivity and performance of a new improved design portable asymmetrical solar still utilizing thermoelectric modules, Energy Convers. Manage. 118 (2016) 55-62.
[29] S. Danish, A. El-Leathy, M. Alata, H. Al-Ansary, Enhancing Solar Still Performance Using Vacuum Pump and Geothermal Energy, Energies 12 (2019) 539.
[30] A. Bilgil, B. Hırlakoğlu, An experimental study on desalination at vacuum environment under low pressure and low condensation temperatures, Desalination 411 (2017) 9-18.
[31] L. Zhu, R.F. Boehm, Y. Wang, C. Halford, Y. Sun, Water immersion cooling of PV cells in a high concentration system, Sol. Energy Mater. Sol. Cells 95 (2011) 538-545.
[32] A. Kheirabadi, D. Groulx, Cooling of server electronics: A design review of existing technology, Appl. Therm. Eng. 105 (2016) 622-638.
[33] G. Xie, W. Chen, T. Yan, J. Tang, H. Liu, S. Cao, Three-effect tubular solar desalination system with vacuum operation under actual weather conditions, Energy Convers. Manage. 205 (2020) 112371.
[34] A. Qandi, I. Alshaikh, N. Aljabarin, K. Rababa, N. Beithou, Analysis of Partially Evacuated Solar Still System under Jordan Climate, Journal of Ecological Engineering 21 (2020) 1-9.
[35] A.G.M. Ibrahim, I. Dincer, A solar desalination system: Exergetic performance assessment, Energy Convers. Manage. 101 (2015) 379-392.
[36] E. Kabeel, Z. Omara, F.A. Essa, Improving the performance of solar still by using nanofluids and providing vacuum, Energy Convers. Manage. 86 (2014) 268-274.
[37] L. Huang, H. Jiang, Y. Wang, Z. Ouyang, W. Wang, B. Yang, H. Liu, X. Hu, Enhanced water yield of solar desalination by thermal concentrated multistage distiller, Desalination 477 (2020) 114260.
[38] G. Wu, Q. Yang, H. Zheng, Y. Zhang, H. Fang, R. Jin, Direct utilization of solar linear Fresnel reflector on multi-effect eccentric horizontal tubular still with falling film, Energy 170 (2019) 170-184.
[39] S. Okamoto, S. Seo, K. Nakaso, I. Kawai, Turbulent Shear Flow and Heat Transfer Over the Repeated Two-Dimensional Square Ribs on Ground Plane, Journal of Fluids Engineering 115 (1993)

631-637.
[40] Y.h. Xie, H. Yang, Q.t. Ma, Evaluation of Solar Energy Resources in Xichang, Electric Power Survey & Design (2010) 06.
[41] S. Kline, Describing uncertainty in single sample experiments, Engineering 75 (1953) 3-8.
[42] Suntask Inc. Daily efficiency of solar collector. http://www.suntask.com/index.php?ac=article&at=read&did=74. [access date 23/10/2020]
[43] S. Rastegar, H. Kargarsharifabad, N. Rahbar, M.B. Shafii, Distilled water production with combination of solar still and thermosyphon heat pipe heat exchanger coupled with indirect water bath heater – Experimental study and thermoeconomic analysis, Appl. Therm. Eng. 176 (2020) 115437.
[44] M.S. Yousef, H. Hassan, Energetic and exergetic performance assessment of the inclusion of phase change materials (PCM) in a solar distillation system, Energy Convers. Manage. 179 (2019) 349-361.
[45] P. Taheri, A.R. Zahedi, Techno-economic analysis of a renewable quadruple hybrid system for efficient water/biofuel production, Sol. Energy 211 (2020) 1053-1069.
[46] F. Alshammari, M. Elashmawy, M.M.Z. Ahmed, Cleaner production of freshwater using multi-effect tubular solar still, J Clean Prod 281 (2021) 125301.
[47] H.E.S. Fath, M. El-Samanoudy, K. Fahmy, A. Hassabou, Thermal-economic analysis and comparison between pyramid-shaped and single-slope solar still configurations, Desalination 159 (2003) 69-79.
[48] M. Elashmawy, M. Alhadri, M.M.Z. Ahmed, Enhancing tubular solar still performance using novel PCM-tubes, Desalination 500 (2021) 114880.
[49] M.E.H. Attia, A.E. Kabeel, M. Abdelgaied, F.A. Essa, Z.M. Omara, Enhancement of hemispherical solar still productivity using iron, zinc and copper trays, Sol. Energy 216 (2021) 295-302.
[50] M. Estahbanati, M. Feilizadeh, K. Jafarpur, M. Feilizadeh, M. Rahimpour, Experimental investigation of a multi-effect active solar still: The effect of the number of stages, Appl. Energy 137 (2015) 46-55.
[51] Z.M. Omara, E. Kabeel, F.A. Essa, Effect of using nanofluids and providing vacuum on the yield of corrugated wick solar still, Energy Convers. Manage. 103 (2015) 965-972.
[52] A. Ibrahim, E. Allam, S. Elshamarka, A modified basin type solar still: Experimental performance and economic study, Energy 93 (2015) 335-342.
[53] S.W. Sharshir, N. Yang, G. Peng, E. Kabeel, Factors affecting solar stills productivity and improvement techniques: A detailed review, Appl. Therm. Eng. 100 (2016) 267-284.
[54] G.N. Tiwari, L. Sahota, Review on the energy and economic efficiencies of passive and active solar distillation systems, Desalination 401 (2017) 151-179.
[55] G. Xie, L. Sun, T. Yan, J. Tang, J. Bao, M. Du, Model development and experimental verification for tubular solar still operating under vacuum condition, Energy 157 (2018) 115-130.
[56] K. Srithar, T. Rajaseenivasan, Recent fresh water augmentation techniques in solar still and HDH desalination – A review, Renewable Sustainable Energy Rev. 82 (2018) 629-644.
[57] A. Ahsan, T. Fukuhara, Mass and heat transfer model of Tubular Solar Still, Sol. Energy 84 (2010) 1147-1156.
[58] W. Henry, Heat transmission, McGraw-Hill, New York, 1954.
[59] C.O. Popiel, J. Wojtkowiak, Simple Formulas for Thermophysical Properties of Liquid Water for Heat Transfer Calculations (from 0°C to 150°C), Heat Transf Eng. 19 (1998) 87-101.

[60] V.T. Morgan, The overall convective heat transfer from smooth circular cylinders, Adv Heat Transf 11 (1975) 199-264.